RSC Applied Polymers

ROYAL SOCIETY OF CHEMISTRY

PAPER

View Article Online
View Journal | View Issue

Cite this: *RSC Appl. Polym.*, 2025, **3**, 722

Interfacial stress transfer in graphene-based polymeric inks on a textile surface for long term cycling stability

Monika Swami,†[a,b] Shanu Prabhakar,[a,c] Susanta Ghosh [b] and Debmalya Roy *[a]

The viscosity of graphene-based conducting ink has been shown to significantly affect printed geometries, and it has been illustrated that it can be controlled by adjusting the crosslinking density. A porous substrate, such as a textile surface, has been selected for printing to emphasize the structure formation of nanofillers during cyclic bending. The graphene loading in the elastomer matrix was deliberately chosen beyond the percolation threshold to gain insight into the conducting network channels on the fabric substrate. Structure–property analysis revealed the formation of stable conducting geometries of graphene on textile yarns under cyclic stress. The processing parameters have been found to play a crucial role in fabricating a tightly packed, conducting ink-filled textile substrate, which reorganizes the structural integrity of the flexible film by application of stress. The flexibility of graphene flakes is found to be critical as it allows them to conform to the fabric's surface for enhanced wetting and to minimize the stress concentration. The composition of fabric materials plays an important role in enhancing adhesion with conducting layers, thus contributing to the overall resistance stability. Formulation and processing of graphene-based inks have been optimized to achieve consistent deposition of flexible conductive ink on textile surfaces capable of enduring bending stress, making it ideal for the next generation of wearable electronics applications.

Received 18th September 2024,
Accepted 26th March 2025

DOI: 10.1039/d4lp00289j

rsc.li/rscapplpolym

1. Introduction

The development of stretchable conducting materials with high cycling stability is a significant challenge in materials science and engineering, particularly for flexible electronic devices. Wearable electronics require materials that can withstand repeated stretching and bending without losing their electrical conductivity or mechanical integrity.[1–3] Traditional rigid electronic materials, such as silicon or metals, are unsuitable for wearable electronics due to their lack of flexibility and stretchability. Substrates made from these materials can be made conformable in thin films which generally experience sudden electrical disconnection when mechanical deformation occurs, highlighting their limitations in maintaining conductivity under strain. Therefore, lots of efforts have been made in the recent past to explore new materials, fabrication techniques, and substrates to overcome these limitations.[4,5]

The next-generation flexible electronics necessitates the development of materials systems with increased mechanical stabilities and multifunctionalities to cater to the demand of diverse applications.[6,7] Innovative nature-inspired structural designs have provided new concepts for smarter performances during cyclic or geometrical deformation to fabricate skin-attachable sensors. Equal attention has been focused on the development of a low-cost enabling platform like paper or textile for printable electronics where lots of efforts have been made to optimize the process of deposition of materials to address the issues of permeating the substrate.[8–10]

In the last couple of decades, the field of electronics has witnessed a transformative breakthrough with the emergence of graphene.[11,12] One of the most promising applications of graphene lies in flexible electronics, where its exceptional flexibility, transparency, electrical conductivity, and mechanical strength make it a unique choice. The advantage of graphene-based flexible electronics is their ability to bend, twist, and conform to different shapes without losing functionality and structural integrity.[13] Unlike the other allotropes of carbon like 1D carbon nanotubes and 0D fullerenes/nanoparticles, 2D graphene has witnessed surface corrugations and crumples under

[a]*Nanoscience & Coating Division, DMSRDE, GT Road, Kanpur 208013, India. E-mail: droy.dmsrde@gov.in*
[b]*Integrated Science Education & Research Centre, Visva-Bharati University, Santiniketan-731235, India*
[c]*Department of Textile Technology, Uttar Pradesh Textile Technology Institute, Kanpur-208001, India*
†Current Address: Department of Electrical & Computer Engineering. Northeastern University 360 Huntington Ave, Boston, MA 02115.

stress due to a significantly higher available cross-sectional area.[14] Due to these unique wrinkles and ripples of 2D flakes under stress, the graphene-based polymeric inks give rise to the opportunity to control the orientation of 2D configurations in ink medium. It has been found that the ink formulation and nature of the substrate influence the properties of large-area printing due to the self-assembled morphology of 2D flakes during drying of graphene films.[15,16] The viscosity and surface tension of the colloidal dispersion of 2D materials are even more critical for constant jetting from all nozzles during inkjet printing. The resistance of digitally printed graphene-based thin films can be tuned by controlling the post-annealing conditions where the 2D lamellas form interconnected networks.[17,18] The printing of graphene inks by more economical screen printing or a more advanced version of 3D printing has also been reported where the intrinsic conductivity and exfoliated geometry of 2D flakes affect the properties and performance of printed patterns.[19,20]

Long-term stability of printed graphene films without a significant degradation in conductivity is crucial and the intrinsic conductivity of carbonaceous nanomaterials plays a critical role. A one atom thick crystalline graphite sheet shows very high electrical conductivity; however, its scalability, processability, and cost have been the major implications for the successful large-scale use of single-layer graphene.[21,22] 2D carbonaceous materials prepared using the chemical method are easier to produce; however, graphene oxide (GO) exhibits lower electrical conductivity compared to defect-free graphene sheets. The oxygenated functional moieties on the graphene flakes help disperse them in the polymer matrix, however creating defects in the hexagonal lattice which reduces the charge mobilities. The partial reduction of GO to restore the sp^2 carbon structure results in enhanced conductivities in reduced graphene oxide (rGO) with better flexibility, mechanical strength, and improved chemical stability. The ability to control the functional moieties and defects in the carbon lattice provides the opportunity to generate specific properties contributing to its appeal in scientific research and particularly for synthesizing conducting inks for printing.[23,24]

The substrate is a critical building block in printing technologies, significantly influencing the success of the entire manufacturing process. Its flexibility adds a crucial dimension for creating bendable and conformable electronic circuits, where surface properties directly impact the printability and adhesion of conducting inks. A wide range of flexible substrate materials is commonly used in printed electronics, offering diverse options to meet specific application needs.[25] Polyethylene terephthalate (PET) is a popular choice for flexible substrates due to its transparency, high mechanical strength, and dimensional stability. On the other hand, polyimide (PI) or polyethylene naphthalate (PEN) were often used when thermal stability and chemical resistance were the determining factors for flexible circuits. Paper and paper-based substrates offer environmentally friendly and cost-effective alternatives, finding application in disposable electronics and smart packaging. The inherent flexibility of textiles allows for the creation of wearable electronics where sensors, conductive inks, and even microelectronics can be printed directly onto the fabric.[26–28]

While textile fabric-based printable electronics hold great promise for wearable technology, they also face significant challenges. One of the primary issues is maintaining the mechanical properties and breathability of the fabric while integrating electronic components. As the ink comes in contact with the textile surface, diffusion takes place, allowing the conducting particles to spread and embed themselves within the fabric matrix. The diffusion process not only determines the functionality of the printed conductive elements but also plays a pivotal role in ensuring the durability and longevity of the printed design on the textile substrate. The intricate interplay between the ink and textile surface influences the final electrical and mechanical properties of the printed pattern, making it essential for applications ranging from electronic textiles to wearable technology.[29,30]

In this work, we report a unique method for graphene-based ink formulation by generating pre-crosslinked graphenes before adding polymeric additives. Pre-curing with a crosslinking agent ensures that the graphene flakes are exfoliated to address the sedimentation of conducting fillers. This study establishes that textile cloth stands out as an excellent option for conferring flexibility and long-term cycling stability to printed geometries. It has been illustrated that the post-curing of printed rGO based inks on textile yarns resulted in enhanced wetting, fostering the generation of interpenetrating conducting channels. The repeated application and release of bending stress on the printed textile fabrics validate that rGO gel-based ink on textile surfaces holds promise as a solution for sustained conductivity in printed patterns by controlling the interfacial interactions. This study may have a significant impact on the formulation and material selection in the manufacturing of flexible electronic circuits printed on textile surfaces, thereby contributing to the advancement of wearable sensors for healthcare monitoring and various other applications.

2. Experimental

2.1 Materials

Graphite powder with a particle dimension of 20 μm was supplied by Sigma-Aldrich. The other chemicals *viz*. $KMnO_4$ (with a purity of 99%), H_2SO_4 (with a purity of 96%), H_3PO_4 (with a purity of 50%), H_2O_2 (with a purity of 33%), and ascorbic acid were purchased from a local chemical shop and used as received. PDMS (SYLGARDTM 184 Silicone Elastomer Kit) was purchased from Dow Chemical International Private Limited (Dow India). All other chemicals were obtained from the local market and used as received.

2.2 Analyses

The structural analysis of the developed nanomaterials, ink, and the printed surface has been conducted using a SUPRA 40 VP, Gemini, Carl Zeiss scanning electron microscope (SEM).

For morphological and energy-dispersive X-ray spectroscopy (EDX) studies, the nanomaterials were dispersed in alcohol and drop-cast onto double-sided carbon tape to record the SEM images. The geometrical analysis of the flexible films was recorded after initially preparing the free-standing thin films using a doctor's blade with graphene-based inks. As previously described, SEM cross-sectional images of the printed layers on the textile surface were obtained.[31] X-ray diffraction (XRD) of the powder nanomaterial samples was carried out on a Bruker D8 ADVANCE diffractometer within the scanning 2θ range of 5–90 degrees. The GO and rGO powder samples were characterized using Fourier transform infrared (FTIR) spectroscopy (ALPHA II, Bruker, U.S.A.) in the range of 700–4000 cm^{-1} with 32 scans and 4 cm^{-1} resolution in transmission mode by preparing KBr pellets. Contact angle measurements were conducted in sessile drop mode under ambient conditions utilizing the OCA 50 system from DataPhysics Instruments, Germany. The surface topographic images of the samples were recorded on non-contact 3D optical imaging Zeta instruments. The *in situ* electrical resistance of the films was measured using a Keithley, 2700 Multimeter, and a minimum of 03 samples were recorded for statistical averaging. The two-probe method was favoured over the four-probe method, as the latter makes it challenging to repeatedly bend the sample. As outlined in the report, the bending radius of the coated fabrics was periodically varied from 0 and 8.9 mm, corresponding to a bending strain of 1.5%.[32,33] The measurement of the conductivity of flexible films under stress was carried out in an automated bending machine fitted with an electrical resistance measurement system for *in situ* analysis of the physical properties during bending. The analyses were conducted on Kevlar, glass, and polyester fabrics coated with graphene-based inks up to 400 cycles under cyclic bending stress. The films underwent cyclic strain of ±1 mm from their original lengths using a bi-directional stretching device, with a constant strain rate of 0.5 mm s^{-1} consistently applied during the measurements. At the same time, the electrical conductivity of the samples was measured with a Keithley source meter, applying a constant potential of 20 V.

2.3 Synthesis of graphene oxide

Graphene oxide (GO) is synthesized from pure graphite powder using sulfuric acid (27 ml) and phosphoric acid (3 ml, in a 9 : 1 ratio), mixed and stirred. Graphite powder (0.225 g) is added and stirred in this acidic solution. Potassium permanganate (1.32 g) is slowly added, and the mixture is stirred for 6 hours until it turns dark green. To remove excess potassium permanganate, hydrogen peroxide (0.675 ml) is added and stirred for 10 minutes. After cooling, hydrochloric acid (10 ml) and deionized water (30 ml) are added, followed by centrifugation at 5000 rpm for 7 minutes. The supernatant is decanted, and the residue is washed three times with hydrochloric acid and deionized water. Finally, the washed GO solution is dried in an oven at 90 °C for 24 hours to produce GO powder. The process of GO fabrication is schematically described in Fig. 1A.

2.4 Reduced graphene oxide (R-GO) synthesis using L-ascorbic acid

The controlled introduction of functional moieties on graphene flakes is crucial for obtaining dispersibility in a matrix with enhanced conductivity.[34,35] 4 g of GO is dispersed in 100 ml of distilled water and sonicated for 1 h. After the sonication, 80 mg of L-ascorbic acid is mixed in the solution and stirred for 2.5 h at 90 °C, maintaining a pH of 7. The ratio of the reducing agent to GO and the reaction time were systematically optimized. Consequently, GO was effectively reduced using ascorbic acid to yield reduced graphene oxide (rGO). A typical rGO production method is illustrated in Fig. 1B.

2.5 Preparation of graphene-based inks

Printing ink based on rGO was formulated by incorporating PDMS (SYLGARD™ 184) as an elastomeric matrix. The process has been optimized to eliminate larger-sized rGO flakes that tend to settle out of the ink. In the first step, reduced graphene oxide (rGO) flakes were dispersed in toluene by sonication, after which a few drops of hydroxylated polydimethylsiloxane (PDMS) were added. Following this, reduced pressure distillation was employed to evaporate the excess organic solvent, leading to the formation of a viscous rGO crosslinked gel. PDMS was subsequently added dropwise to the rGO gel while maintaining continuous stirring at an elevated temperature of 80 °C. The stirring is continued until a homogeneous solution is obtained, which can be stored for a few days without any observable settling of 2D flakes. The curing agent was introduced in a slightly higher ratio (1 : 0.12) as prescribed, and it was uniformly mixed with the ink using a vacuum-speed mixture.[6,33] The viscosity of the resulting ink was slightly reduced after the addition of the curing agent, making it suitable for printing on textile surfaces. However, the final ink needed to be used within 6 hours of adding the curing agent

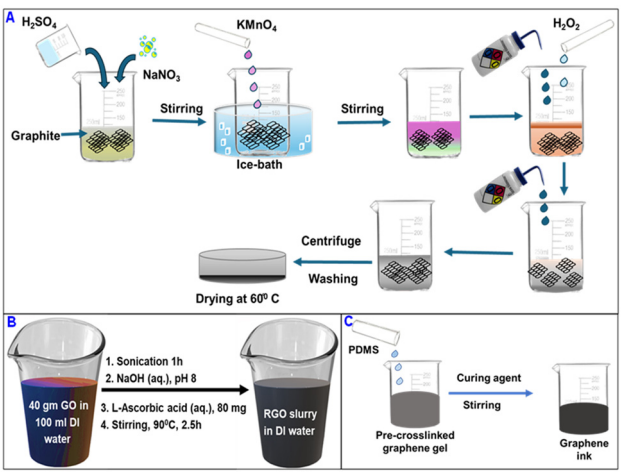

Fig. 1 The modified Hummers' method (A) has been adapted to synthesize GO whereas the process for synthesizing reduced graphene oxide (B) from GO is schematically shown in B and the formulation of the graphene-based ink recipe has been described in C.

due to the observed viscosity build-up over time. The process of graphene ink formulation has been represented in Fig. 1C.

2.6 Printing of graphene-based inks on the textile surface

A thin conducting and flexible layer (500–1000 μm) was printed on 4″ × 4″ plain woven fabrics made of polyester, fiberglass, and Kevlar cloth with 60–75 GSM using an automatic motorized film applicator as shown in Fig. 2. In a typical process, 5.0 ml of graphene ink was dispensed onto the applicator, and the thickness was adjusted to get the desired thickness of the layer. The ink was then printed onto a clean textile surface and positioned over a glass slide, using a doctor's blade at room temperature. The low GSM of the fiber was utilized to prevent ink diffusion through gaps in the woven surface of the textile yarns. The rGO weight fraction in the elastomer matrix has been varied to understand the interfacial bonding of graphene-based ink with the textile surface. To optimize the printed graphene-based flexible conducting film, the ink was additionally directly printed to a glass slide and subsequently peeled off post-curing to obtain a free-standing film. The printed fabrics were annealed at 120 °C for a duration of 2 h in a vacuum oven to get the final printed fabrics.

3. Results and discussion

3.1 Crosslinking graphene with polymeric precursors for improving dispersion of flakes

The crumpled and folded structure of graphene flakes within the elastomer matrix, along with its two-dimensional form, is critical for achieving the dispersity, conductivity, and stability necessary for graphene-based printing inks.[33,36] In our previous studies, we have established that the attributes of the initial graphite flakes are pivotal in influencing both the degree of derivatization and the conductivity of the resultant functional graphene.[32,37] XRD and electron microscopy analyses were conducted to optimize the processing parameters for the synthesis of graphene oxide using the modified Hummers' method with highly crystalline graphite powder (Fig. 3). Similarly, reduced graphene oxide was synthesized through the controlled reduction of oxygenated moieties, and

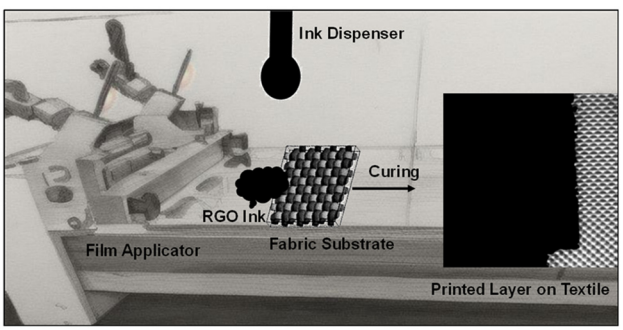

Fig. 2 The process of printing reduced graphene oxide-based ink on a textile surface.

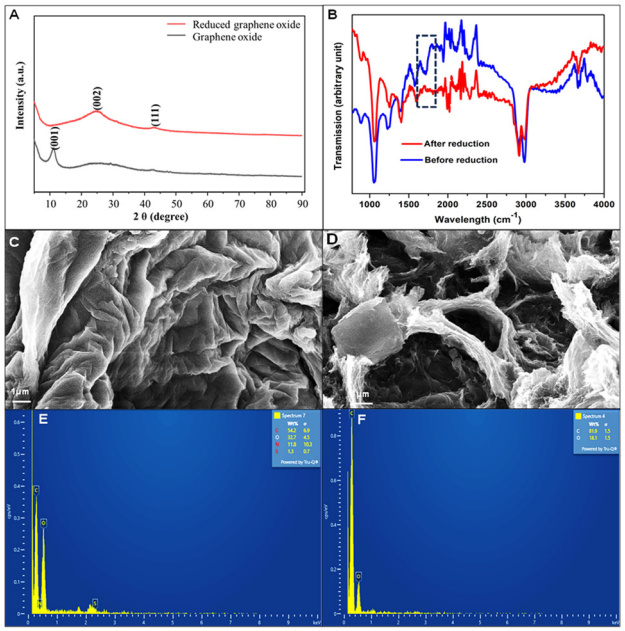

Fig. 3 X-ray diffraction patterns (A), FT-IR spectra (B) before and after reduction of graphene oxide, scanning electron microscopy images (C and D), and energy dispersive X-ray analysis results (E and F) of the developed GO and rGO samples.

XRD (Fig. 3A), FT-IR (Fig. 3B), SEM (Fig. 3C & D), and EDX (Fig. 3E & F) analyses were found to be critical in fine-tuning the processing parameters.

The presence of a characteristic peak at a 2θ of 10.2 in GO and the subsequent disappearance of this peak, accompanied by the emergence of a peak around 2θ of 22.0 in rGO, confirm the formation of a crystalline lattice in rGO (Fig. 3A). The FT-IR spectra for both GO and rGO obtained using L-ascorbic acid provide clear evidence of the reduction process and the changes in functional groups. Typically, GO exhibits peaks corresponding to oxygen-containing groups, such as hydroxyl (O–H) stretching vibrations around 3432 cm^{-1} and carbonyl (C═O) stretching vibrations around 1711 cm^{-1}.[38] Upon reduction to rGO, the carbonyl peaks almost disappeared, and the intensity of hydroxyl functional moieties decreases, indicating the substantial removal of oxygenated functionalities from graphene flakes and the restoration of the crystalline graphitic structure in rGO (Fig. 3B). The changes in the morphological properties observed in the SEM images of GO and rGO suggest a pronounced shift in interfacial interactions following the controlled reduction of oxygenated species (Fig. 3C and D). The substantial shift in the carbon-to-oxygen ratio observed in the energy-dispersive X-ray (EDX) spectrum before and after the reduction of GO confirms that our process is optimized to produce 2D nanofillers of enhanced conductivity with dispersibility in the polymer matrix (Fig. 3E and F). This transformation is indicative of higher conductivity and improved dispersity of rGO in the PDMS matrix.[39,40]

The settling of graphene flakes poses a significant challenge when dispersing rGO in an elastomeric matrix, particu-

larly at higher loadings.[41] To address this issue, we have pre-crosslinked graphenes before adding polymeric additives to formulate the conducting ink. Pre-curing ensures that the graphene flakes are exfoliated which reduces the amount of graphene used to reach the percolation threshold.[42] It has been reported that boron interacts with oxygenated species of graphene oxide and can enhance the viscosity of the elastomeric matrix through increased interfacial interactions.[43] This enhancement is crucial for achieving a uniform and continuous deposition of ink made of graphene which improves adhesion and prevents issues such as ink bleeding or spreading during the printing process. A facile method has been developed to prepare a gel of rGO (Fig. 4A) by crosslinking it with hydroxylated PDMS (PDMS-OH) before integrating it into the final PDMS matrix (Fig. 4B). To crosslink graphene flakes with controlled functional moieties to a hydroxyl-functionalized base matrix, *i.e.*, PDMS, crosslinkers such as polyboric acid (boric acid heated in air) have been utilized. Rheological studies (Fig. 4C) indicate that a pinch of boric acid as a crosslinker further increases the viscosity of the resultant PDMS-rGO ink before the addition of a curing agent. The ratio of PDMS-OH to rGO was found to be optimized at 1 : 10 where the lower viscosity (75 cP) of PDMS-OH produced a higher crosslinking density.[44]

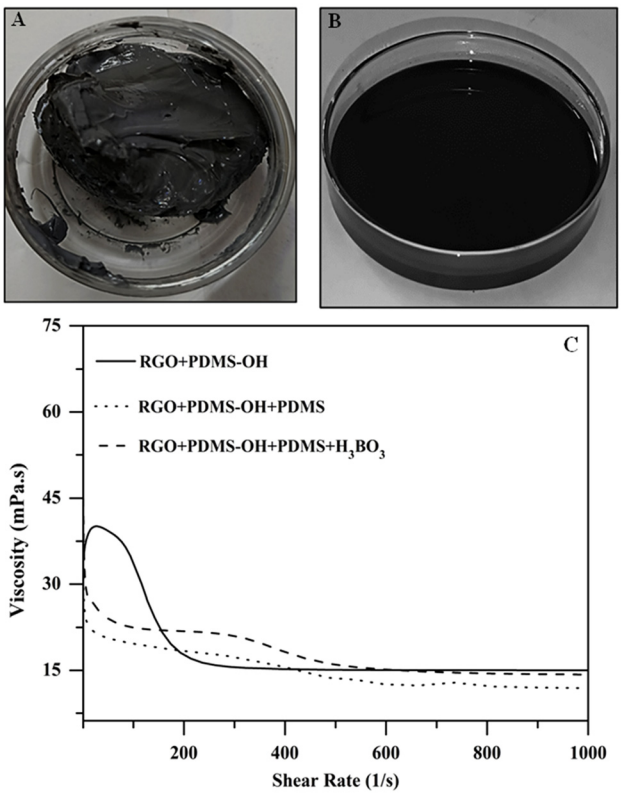

Fig. 4 The images of the hydroxyl PDMS crosslinked rGO gel (A) and the corresponding ink (B) after adding PDMS and the curing agent. The rheological studies of different variants of rGO-reinforced materials are represented in C.

The water contact angle of the rGO-reinforced PDMS-OH film has been systematically reduced with the increase in the loading fraction of rGO (Fig. 5A–D). The decrease in contact angle with the increase in conducting nanofiller weight percentage can be attributed to the inherent hydrophilicity of graphene with controlled functionalization in a hydroxylated PDMS matrix. Despite the intrinsic hydrophobic nature of PDMS, the incorporation of rGO enhances the overall hydrophilicity of the resulting composite ink. A higher loading fraction of nanofillers has been previously shown to induce surface roughness in structures formed from a flexible polymer matrix.[45] This roughness generally increases the actual contact area between the liquid and the solid, thereby amplifying the surface's intrinsic wettability. In the case of a hydrophilic surface, the increased roughness allows the liquid to penetrate surface asperities, resulting in a lower contact angle. The contact angle measurement of the PDMS nanocomposite film confirms that incorporating rGO makes the ink hydrophilic, thereby improving its compatibility for enhanced interfacial bonding with the substrate. The reduction in static water contact angle of PDMS from 800 (Fig. 5A) to 41.90 after adding 20% rGO (Fig. 5D) further validates the fact that introducing graphene flakes into the elastomeric matrix results in a more textured and conducting surface, resulting in a decreased contact angle (Fig. 5).[46] The steady decrease in the tilt-base angle observed in both receding and advancing contact angle measurements during dynamic contact angle analysis indicates that a higher rGO loading in ink formulation enhances the roughness of the printed surface, leading to greater adhesion with the textile yarns.

To achieve kiloohm-range resistance for the printed flexible film, the reduced graphene oxide (rGO) loading was adjusted to 10%, 15%, and 20% by weight relative to polydimethylsiloxane. The doctor's blade method, as previously outlined, was employed

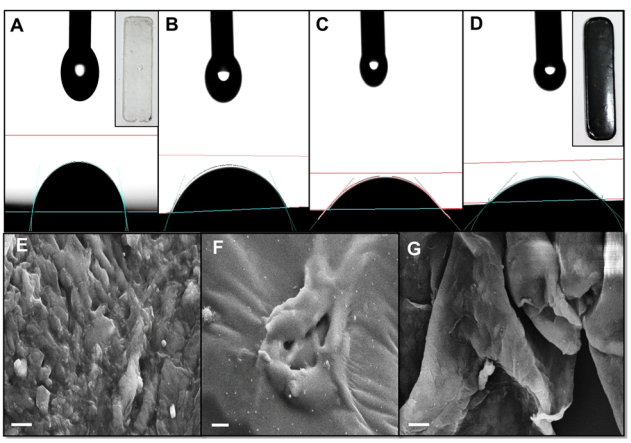

Fig. 5 The water contact angles of the rGO-based film of PDMS (A), 10% (B), 15% (C), and 20% (D) loading are observed to be 80°, 61.1°, 52.1°, and 41.9° whereas the actual free-standing PDMS and nanocomposite film are shown in the inset of the figure. The cross-sectional SEM images of film 10% (E), 15% (F), and 20% (G) loadings are presented (scale bar is 1 μm) in Fig. E–G.

to fabricate free-standing PDMS nanocomposite films with a thickness of 500 μm.[47] The current values obtained at 20 V exhibited a systematic increase corresponding to the loading of rGO, ranging from 0.1 μA to 7.8 μA for 10% and 20% loading where the percolation threshold for device-grade films was identified at 15% reinforcement with our developed rGO gel. SEM images depicting the cross-sections of various nanocomposite films (Fig. 5E–G) serve as direct evidence for the establishment of durable conducting channels with increased loading of 2D flakes. However, it can be noted that at higher loadings, storage modulus values decreased, adversely impacting the flexibility of films for stretchable applications.

3.2 Effect of substrate geometry on electro-mechanical characteristics

To choose an appropriate printing substrate that offers prolonged stability in conductivity and mechanical strength under cyclic stress, our focus shifted to this task after finalizing the optimization of material and processing parameters for the graphene-based ink. Plastic, paper, and textile surfaces are frequently preferred as printing substrates for flexible applications due to their versatility and compatibility with a variety of materials.[25,41] The porous structure of cloths can absorb inks, leading to spreading and diffusion, posing a significant challenge for achieving high-resolution patterns during printing. However, achieving successful printing on textile surfaces is of utmost importance for the advancement of wearable sensors in healthcare monitoring and other applications.[29,44] To investigate the influence of yarn dimensions on the degree of diffusion of viscous fluid, inks were applied to Kevlar fabric of 75 (Fig. 6A) and 300 (Fig. 6B) GSM using the doctor's blade method. The 3D optical microscopy images of the back side of the print fabric distinctly revealed that penetration of the printing ink is less pronounced in the lower GSM cloth which could be attributed to the lower porosity in finely woven Kevlar fibers.

The application of inks on the textile surface followed by annealing to cure the film significantly impacted the morphology of the printed layers. In organic solar cells, post-annealing has been observed to create a more uniform and smoother topographic surface, thereby enhancing the mobilities of charge carriers.[48] Here, we emphasize the significance of post-processing annealing in creating high-performance printed films on textile fabrics. The surface (Fig. 6C & E) and 3D topographic (Fig. 6D & F) images obtained before and after annealing at 120 °C for 2 h revealed that the curing process of flexible conducting films resulted in a smoother layer with improved physical properties. The curing kinetics of inks based on rGO were observed to follow the pattern exhibited by functionalized CNTs in the PDMS matrix, a process that we have optimized to achieve higher mechanical and electrical properties in free-standing films.[5]

3.3 Influence of substrate physicochemical properties on sustained properties

The printing of rGO inks on varied textile surfaces like Kevlar, fiberglass, and polyester cloths with 75–60 GSM was carried out using an automatic motorized film applicator. The selection of Kevlar, glass, and polyester fabric has been made to ensure the broadest possible range of options, with Kevlar fabric being untreated, glass fabric treated with a silane sizing element, and polyester fabric featuring built-in functionalities. The surface images of printed cloth of Kevlar (Fig. 7A), fiberglass (Fig. 7B), and polyester (Fig. 7C) revealed that rGO ink can be applied to any textile surface, highlighting the distinctive formulation of the pre-crosslinked ink. In the 3D surface topographic images of the printed layers with 10% (Fig. 7D & G), 15% (Fig. 7E & H), and 20% (Fig. 7F & I) of pre-crosslinked rGO-based inks, it has been observed that over the higher loading of percolation threshold, rGO leads to the precipitation of graphene flakes on the fibers. We aim to emphasize the critical role of loading percentage, as excessive conducting filler compromises the stability of printed layers on textile yarns, adversely affecting the overall performance of the flexible conductive layer.

To further investigate the structure formation of rGO fractals in the printed layer and to get insight into the interfacial geometry of graphene flakes and textile yarns, SEM studies of the cross-section of the printed film were conducted (Fig. 8). The interfacial geometry between textile fibers and the elastomer matrix reinforced with rGO varied among Kevlar (8A), fiberglass (8B), and polyester (8C). This variation suggests that the surface treatment of yarns plays a crucial role in influencing the performance of printed layers on fabrics. For a deeper understanding of the bonding between fabrics and printed

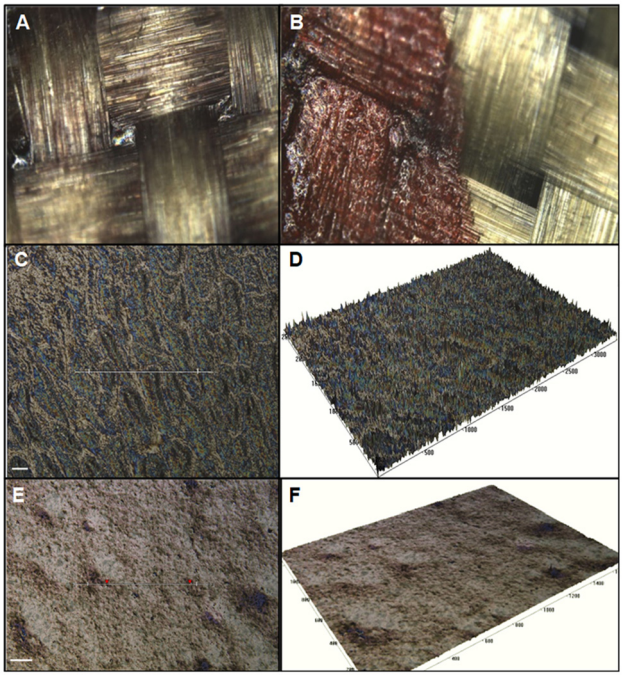

Fig. 6 The 3D optical images of the non-contact mode of the back side of the printed layers on 75 (A) and 300 (B) grams per square metre (GSM) Kevlar fabric. The surface (C and E) and topographic (D and F) images of the printed textile surface before and after annealing respectively where the scale bar is 150 μm.

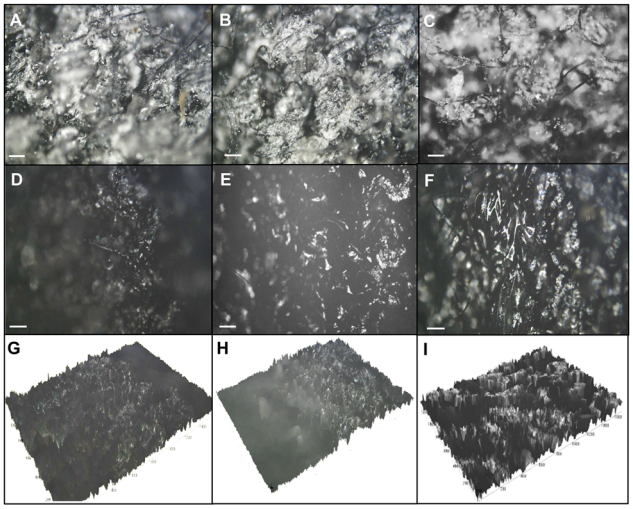

Fig. 7 The optical images of the printed layers using 15% rGO inks on Kevlar (A), fiberglass (B), and polyester (C) cloths respectively. The surface and 3D topographic images of films were obtained by printing 10% (D & G), 15% (E & H), and 20% (F & I) rGO-based inks where the scale bar is 150 μm.

layers, the interfacial boundaries of individual textile yarns and the PDMS modified with graphene flakes were examined using high-resolution SEM images. In a manner analogous to the findings in photovoltaic layers, annealing was observed to enhance the compactness of interlaced yarns within the fabric through co-curing with 2D lamellar nanofiller-reinforced elastomers (Fig. 8D & E).

The closely packed interfacial microstructures between textile fabrics and rGO ink represent an ideal platform for absorbing the residual stress generated in the system by the application of cyclic loads [Fig. 9A].[49] To assess the stability of these densely packed network geometries, we measured the change in resistance of the printed monolayer of ink by repeated bending of the film with a radius of 8.9 mm, corresponding to a 1.5% bending stress.[35] It is worth mentioning that a 0.5 mm single layer of this printed geometry exhibited resistance comparable to that of six layers of conducting ink printed on e-textiles.[50] It can be noted that at lower filler loadings (Fig. 8F), the resistance values increase sharply with cyclic load which could be attributed to the weak interfacial interactions in the irregular agglomerates of graphene flakes below the percolation threshold.[33] At a higher volume fraction loading of 2D nanofillers (Fig. 8F), the reduction in resistance is found to be less significant after bending, suggesting the unfolding of twisted lamellar geometries of graphene under stress.[45] This enables efficient transfer of external force to the textile yarns, facilitating the formation of stable interpenetrating conduction channels with graphene-based inks. The sustained conductivity of the printed geometries on the textile surface after 10 bending cycles of the film affirms that the combination of graphene flakes' fractals and strong interfacial adhesion with yarns has the potential to meet the criterion of maintaining unaltered electrical conductivity under repeated

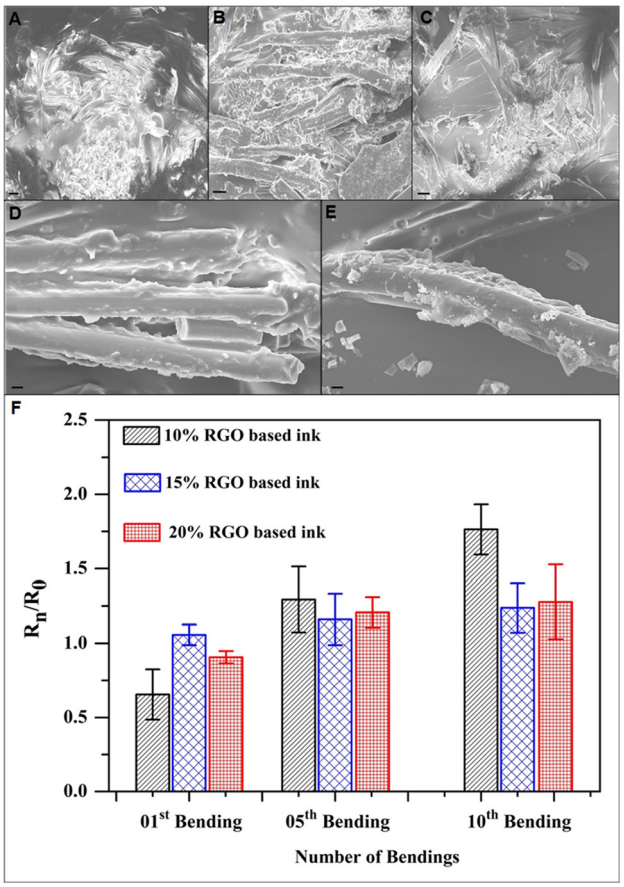

Fig. 8 SEM images of the cross-section of 15% rGO ink printed on Kevlar (A), fiberglass (B), and polyester (C) fabrics. The interfacial bonding of polyester yarns and 15% rGO ink is illustrated before (D) and post (E) annealing at 120 °C for 2 h where the SEM scale bars are 20 (A–C) and 2 (D and E) μm, respectively. The change of resistance of the different weight fraction rGO-based inks on polyester fabric has been represented where R_n and R_0 indicate the resistance value before and after nth bending is represented in (F).

cyclic stresses. The slightly higher conductivity observed after a few bending cycles suggests the realignment of intermolecular network geometries of graphene flakes within the elastomer matrix. This realignment, induced by applied stress, contributes to the formation of a more stable, monolithic fabric-reinforced printed flexible film.[51] Our studies have established that the appropriate volume fraction of 2D flake fractals in stretchable matrix, ink microstructures along with integrated textile yarns provides suitable flexibility to fabricate wearable sensors for niche technological applications.

3.4 Role of mechano-electrical stability

To understand the impact of various textile surfaces on the long-term stability of conduction channels within the embedded ink-infused textile cloth, we selected three cloths exhibiting diverse properties. An automated stepper motor-controlled device has been fabricated, featuring all necessary electrical contacts, to generate bending stress for *in situ*

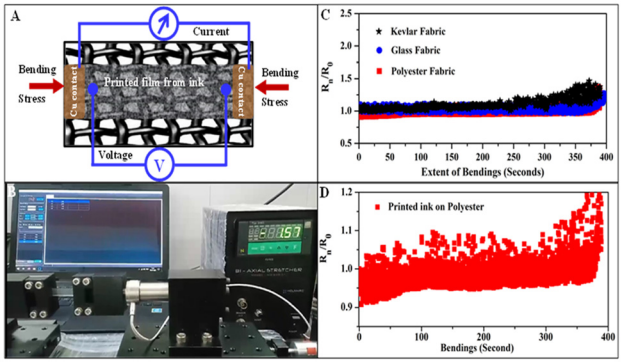

Fig. 9 The schematic (A) and the actual instrument (B) fabricated for the automated bending of flexible films fitted with electrical resistance measurement for *in situ* analysis of conductivity under stress. The stabilities of conduction networks in graphene-based films on Kevlar, glass, and polyester fabrics have been tested under cyclic bending stress for up to 400 seconds where a total of 2 seconds is required to complete each bending cycle. Figure (C) represents the R_n/R_0 values of printed inks on the textile surface and figure (D) illustrates the expanded region of change in resistance of the printed ink on the polyester fabric where the sampling rate is 15 data per second. The cloths were subjected to a cyclic strain of (±)1 mm from their nominal lengths using a bidirectional stretching device with a constant strain rate of 0.5 mm per second maintained throughout the measurements. Simultaneously, the electrical conductivity of the samples was recorded using a Keithley source meter by applying a constant potential of 20 V.

measurement of conductivity under cyclic force (Fig. 9A and B). The high-performance synthetic Kevlar fabric is made of *para*-aramid and is generally used for heat-resistant and blast protection applications and glass fabric finds more widespread use in reinforcing polymer composites for structural applications.[52,53] The electrical resistivity of printed films on both Kevlar and glass fabrics indicates that the silane-based coating on glass fiber yarns further assists in stabilizing graphene-based inks on the glass fabric, contrasting with Kevlar, which exhibits high chemical inertness (Fig. 9C). The characteristics of polyester fabric are its exceptional durability, breathability, and its ability to retain its flexibility ensuring textiles maintain a smooth appearance even after prolonged use.[54] The resistance values of printed graphene inks on polyester fabric illustrate that the fabric's porosity and strong polarity contribute to enhanced adhesion and retained graphene conduction channels through sustained stress transfer within the polyester fabric [Fig. 9D]. Graphene-based inks diffused into textile surfaces are thoroughly engineered to integrate electronic components into fabric structures, providing a lightweight, flexible, and comfortable platform to revolutionize the landscape of wearable electronics and smart textiles.

4. Conclusion

This research emphasizes the significance of carefully controlled reduction of graphene oxide to attain the targeted conductivity, dispersion, and effective interaction with the elastomer matrix. A facile method involving the utilization of hydroxylated PDMS to crosslink graphene flakes before their introduction into the PDMS matrix has been implemented to enhance the possibility of the formation of a more effective conduction network. It has been established that the post-curing process of printed layers on fabrics results in the integrated morphology of textile yarns and graphene flakes, facilitated by elastomeric binders. The interpenetrating closely packed interfacial geometry has been demonstrated to be ideal for absorbing bending stress and maintaining conducting channels even after repeated cyclic stress. The structural analysis and cyclic resistance measurements suggest that optimal graphene loading and fractal morphologies are crucial for sustained conductivity, making this approach advantageous for developing durable wearable electronics.

Data availability

The bending data for this article are available at the Scientist Data Bank at DOI: **https://www.scidb.cn/en/s/Z7jm22**.

Conflicts of interest

There are no conflicts to declare.

Acknowledgements

The authors acknowledge the help from Mr Sudhanshu Singh, Mr Sudhanshu Tiwari, and Mr Dular Chand Bharti, DMSRDE for performing XRD, optical imaging, and contact angle analyses. The authors gratefully acknowledge Dr Prabhat Dwivedi, IIT, Kanpur for helping in recording cross-sectional SEM images. One of us (MS) acknowledges the Department of Science & Technology (DST), Government of India for the DST INSPIRE Fellowship. The authors also thank Dr Kingsuk Mukhopadhyay and Mr Subhash Mandal, DMSRDE for fruitful discussions and suggestions. The authors acknowledge the help from the Department of Physics, Applied Science cluster, UPES, Dehradun, for recording the change of resistance of the film under cyclic bending stress. The authors appreciate the assistance and support extended by the scientists, research scholars, and staff members of the Nanoscience and Coating Division, DMSRDE, Kanpur, in conducting the experiments, performing characterization, and offering valuable suggestions. The authors express gratitude to the Director of DMSRDE, Kanpur, for providing assistance, support, and guidance and granting permission to publish the experimental findings of the master's dissertation research.

References

1 H. Zhao, R. Su, L. Teng, Q. Tian, F. Han, H. Li, Z. Cao, R. Xie, G. Li, X. Liu and Z. Liu, Recent advances in flexible and wearable sensors for monitoring chemical molecules, *Nanoscale*, 2022, **14**, 1653–1669.

2 Y. Liu, M. Pharr and G. A. Salvatore, Lab-on-Skin: A Review of Flexible and Stretchable Electronics for Wearable Health Monitoring, *ACS Nano*, 2017, **11**, 9614–9635.
3 X. Dong, X. Luo, H. Zhao, C. Qiao, J. Li, J. Yi, L. Yang, F. J. Oropeza, T. S. Hu, Q. Xu and H. Zeng, Recent advances in biomimetic soft robotics: fabrication approaches, driven strategies and applications, *Soft Matter*, 2022, **18**, 7699–7734.
4 V. O. Mercadillo, K. C. Chan, M. Caironi, A. Athanassiou, I. A. Kinloch, M. Bissett and P. Cataldi, Electrically Conductive 2D Material Coatings for Flexible and Stretchable Electronics: A Comparative Review of Graphenes and MXenes, *Adv. Funct. Mater.*, 2022, **32**, 2204772.
5 D. Roy, B. Vaishnav, S. K. Vayalil, A. Gupta, N. E. Prasad, B. Sochor, M. Schwartzkopf, S. V. Roth and T. Kraus, In Situ Study of Structure Formation under Stress in Stretchable Conducting Nanocomposites, *J. Phys. Chem. Lett.*, 2023, **14**, 5834–5840.
6 X. Wu, W. Fu and H. Chen, Conductive Polymers for Flexible and Stretchable Organic Optoelectronic Applications, *ACS Appl. Polym. Mater.*, 2022, **4**, 4609–4623.
7 D. Corzo, G. T. Blázquez and D. Baran, Flexible electronics: status, challenges and opportunities, *Front. Electron.*, 2020, **1**, 594003.
8 J. Sun, R. Sun, P. Jia, M. Ma and Y. Song, Fabricating flexible conductive structures by printing techniques and printable conductive materials, *J. Mater. Chem. C*, 2022, **10**, 9441–9464.
9 S. V. Wanasinghe, B. Johnson, R. Revadelo, G. Eifert, A. Cox, J. Beckett, T. Osborn, C. Thrasher, R. Lowe and D. Konkolewicz, 3D printable adhesive elastomers with dynamic covalent bond rearrangement, *Soft Matter*, 2023, **19**, 4964–4971.
10 Y. Yang, S. Duan and H. Zhao, Advances in constructing silver nanowire-based conductive pathways for flexible and stretchable electronics, *Nanoscale*, 2022, **14**, 11484–11511.
11 H. Jang, Y. J. Park, X. Chen, T. Das, M. S. Kim and J. H. Ahn, Graphene–based flexible and stretchable electronics, *Adv. Mater.*, 2016, **28**, 4184–4202.
12 S. M. Cui, S. Hashmi, W. Q. Li, S. H. Wang, C. T. Zhu, S. C. Wang, Y. F. Huang, G. M. Zhu and F. J. Stadler, Rheology of graphene oxide stabilized Pickering emulsions, *Soft Matter*, 2023, **19**, 4536–4548.
13 D. G. Papageorgiou, I. A. Kinloch and R. J. Young, Mechanical properties of graphene and graphene-based nanocomposites, *Prog. Mater. Sci.*, 2017, **90**, 75–127.
14 S. Deng and V. Berry, Wrinkled, rippled and crumpled graphene: an overview of formation mechanism, electronic properties, and applications, *Mater. Today*, 2016, **19**, 197–212.
15 S. Conti, G. Calabrese, K. Parvez, L. Pimpolari, F. Pieri, G. Iannaccone, C. Casiraghi and G. Fiori, Printed transistors made of 2D material-based inks, *Nat. Rev. Mater.*, 2023, **8**, 651–667.
16 E. Jabari, F. Ahmed, F. Liravi, E. B. Secor, L. Lin and E. Toyserkani, 2D printing of graphene: a review, *2D Mater.*, 2019, **6**, 042004.
17 Y. Gao, W. Shi, W. Wang, Y. Leng and Y. Zhao, Inkjet printing patterns of highly conductive pristine graphene on flexible substrates, *Ind. Eng. Chem. Res.*, 2014, **53**, 16777–16784.
18 Y. Lia, Reversible wrinkles of monolayer graphene on a polymer substrate: toward stretchable and flexible electronics, *Soft Matter*, 2016, **12**, 3202–3213.
19 P. He, J. Cao, H. Ding, C. Liu, J. Neilson, Z. Li, I. A. Kinloch and B. Derby, Screen-printing of a highly conductive graphene ink for flexible printed electronics, *ACS Appl. Mater. Interfaces*, 2019, **11**, 32225–32234.
20 K. Hassan, M. J. Nine, T. T. Tung, N. Stanley, P. L. Yap, H. Rastin, L. Yu and D. Losic, Functional inks and extrusion-based 3D printing of 2D materials: a review of current research and applications, *Nanoscale*, 2020, **12**, 19007–19042.
21 P. Bøggild, D. M. A. Mackenzie, P. R. Whelan, D. H. Petersen, J. D. Buron, A. Zurutuza, J. Gallop, L. Hao and P. U. Jepsen, Mapping the electrical properties of large-area graphene, *2D Mater.*, 2017, **4**, 042003.
22 W. Yang and C. Wang, Graphene and the related conductive inks for flexible electronics, *J. Mater. Chem. C*, 2016, **4**, 7193–7207.
23 S. Bi, L. Hou, W. Dong and Y. Lu, Multifunctional and Ultrasensitive-Reduced Graphene Oxide and Pen Ink/Polyvinyl Alcohol-Decorated Modal/Spandex Fabric for High-Performance Wearable Sensors, *ACS Appl. Mater. Interfaces*, 2021, **13**, 2100–2109.
24 A. Ji, Y. Chen, X. Wang and C. Xu, Inkjet printed flexible electronics on paper substrate with reduced graphene oxide/carbon black ink, *J. Mater. Sci.: Mater. Electron.*, 2018, **29**, 13032–13042.
25 M. Hassan, G. Abbas, N. Li, A. Afzal, Z. Haider, S. Ahmed, X. Xu, C. Pan and Z. Peng, Significance of flexible substrates for wearable and implantable devices: recent advances and perspectives, *Adv. Mater. Technol.*, 2022, **7**, 2100773.
26 V. Zardetto, T. M. Brown, A. Reale and A. D. Carlo, Substrates for flexible electronics: A practical investigation on the electrical, film flexibility, optical, temperature, and solvent resistance properties, *J. Polym. Sci., Part B:Polym. Phys.*, 2011, **49**, 638–648.
27 Y. Lin, D. Gritsenko, Q. Liu, X. Lu and J. Xu, Recent Advancements in Functionalized Paper-Based Electronics, *ACS Appl. Mater. Interfaces*, 2016, **8**, 20501–20515.
28 J. S. Heo, J. Eom, Y. H. Kim and S. K. Park, Recent progress of textile–based wearable electronics: a comprehensive review of materials, devices, and applications, *Small*, 2018, **14**, 1703034.
29 H. Ba, L. T. Phuoc, V. Papaefthimiou, C. Sutter, S. Pronkin, A. Bahouka, Y. Lafue, L. N. Dinh, G. Giambastiani and C. P. Huu, Cotton Fabrics Coated with Few-Layer Graphene as Highly Responsive Surface Heaters and Integrated Lightweight Electronic-Textile Circuits, *ACS Appl. Nano Mater.*, 2020, **3**, 9771–9783.
30 N. A. Choudhry, L. Arnold, A. Rasheed, I. A. Khan and L. Wang, Textronics-a review of textile–based wearable electronics, *Adv. Eng. Mater.*, 2021, **23**, 2100469.

31 P. Sayfo, D. Z. Pirityi and K. Pölöskei, Characterization of graphene-rubber nanocomposites: a review, *Mater. Today Chem.*, 2023, **29**, 101397.
32 T. W. Kim, J. S. Lee, Y. C. Kim, Y. C. Joo and B. J. Kim, Bending strain and bending fatigue lifetime of flexible metal electrodes on polymer substrates, *Materials*, 2019, **12**, 2490.
33 Printed Electronics-Part 202-5: Materials-Conductive Ink-Mechanical Bending Test of a Printed Conductive Layer on an Insulating Substrate; IEC 62899-202-:2018; International Electrotechnical Commission: Geneva, Switzerland, 2018.
34 N. Agarwal, R. Bhattacharyya, N. K. Tripathi, S. Kanojia, D. Roy, K. Mukhopadhyay and N. E. Prasad, Derivatization and interlaminar debonding of graphite-iron nanoparticle hybrid interfaces using Fenton chemistry, *Phys. Chem. Chem. Phys.*, 2017, **19**, 16329–16336.
35 V. Agarwal and P. B. Zetterlund, Strategies for reduction of graphene oxide-A comprehensive review, *J. Chem. Eng.*, 2021, **405**, 127018.
36 S. Tkachev, M. Monteiro, J. Santos, E. Placidi, M. B. Hassine, P. Marques, P. Ferreira, P. Alpuim and A. Capasso, Environmentally friendly graphene inks for touch screen sensors, *Adv. Funct. Mater.*, 2021, **31**, 2103287.
37 A. Hudda, S. Singh, S. Tiwari, H. Kumar, A. Vesh, M. Imamuddin, D. Roy and N. E. Prasad, Unravelling the role of nanofillers towards the stability of polymer matrix composite in the marine environment, *Adv. Compos. Mater.*, 2022, **32**, 268–282.
38 M. Palomba, G. Carotenuto and A. Longo, A Brief Review: The Use of L-Ascorbic Acid as a Green Reducing Agent of Graphene Oxide, *Materials*, 2022, **15**, 6456.
39 F. Torrisi, T. Hasan, W. Wu, Z. Sun, A. Lombardo, T. S. Kulmala, G. W. Hsieh, S. Jung, F. Bonaccorso, P. J. Paul, D. Chu and A. C. Ferrari, Inkjet-printed graphene electronics, *ACS Nano*, 2012, **6**, 2992–3006.
40 T. Ge, M. Zhang, K. Tang and H. Tang, Diisocyanate-modified graphene oxide/hydroxyl-terminated silicone rubber composites for improved thermal conductivity, *Mater. Chem. Phys.*, 2020, **252**, 123250.
41 A. Economou, C. Kokkinos and M. Prodromidis, Flexible plastic, paper and textile lab-on-a chip platforms for electrochemical biosensing, *Lab Chip*, 2018, **18**, 1812–1830.
42 D. Roy, B. Vaishnav, S. Mandal, A. Gupta, B. Sochor, S. K. Vayalil and T. Kraus, Origin of Dynamic Network Formation of 2D Nanofillers in Flexible Matrix, *Small Struct*, 2025, DOI: **10.1002/sstr.202400608**.
43 J. Yan, R. Tjandra, H. Fang, L. X. Wang and A. Yu, Boron acid catalyzed synthesis porous graphene sponge for high-performance electrochemical capacitive storage, *Diamond Relat. Mater.*, 2018, **89**, 114–121.
44 G. M. N. Islam, A. Ali and S. Collie, Textile sensors for wearable applications: A comprehensive review, *Cellulose*, 2020, **27**, 6103–6131.
45 S. Prabhakar, J. P. Singh, K. Kumar, S. G. Prasad and D. Roy, Chromium adsorption efficiency by functional polymeric nanocomposite membrane: A case study for environmental sustainability, *Polym. Eng. Sci.*, 2024, **64**, 4774–4785.
46 C. Li, J. Zhang, J. Han and B. Yao, A numerical solution to the effects of surface roughness on water-coal contact angle, *Sci. Rep.*, 2021, **11**, 459.
47 D. Roy, S. Mandal and M. Dwivedi, A Brief Account on Nanomaterials Reinforced Polymer Composites with Sustained Conductivity for Flexible Electronics, *J. Macromol. Sci., Part A:Pure Appl. Chem.*, 2024, **61**(9), 581–591.
48 I. Candan, Enhancement of inverted organic solar cell parameters by post-production annealing process, *Semicond. Sci. Technol.*, 2021, **36**, 115008.
49 S. Gupta, B. McDonald, S. B. Carrizosa and C. Price, Microstructure, residual stress, and intermolecular force distribution maps of graphene/polymer hybrid composites: Nanoscale morphology-promoted synergistic effects, *Composites, Part B*, 2016, **92**, 175–192115008.
50 N. Karim, S. Afroj, A. Malandraki, S. Butterworth, C. Beach, M. Rigout, K. S. Novoselov, A. J. Casson and S. G. Yeates, All inkjet-printed graphene-based conductive patterns for wearable e-textile applications, *J. Mater. Chem. C*, 2017, **5**, 11640–11648.
51 C. Feng, Z. Yi, L. F. Dumée, C. J. Garvey, F. She, H. B. Lin, S. Lucas, J. Schütz, W. Gao, Z. Peng and L. Kong, Shrinkage induced stretchable micro-wrinkled reduced graphene oxide composite with recoverable conductivity, *Carbon*, 2015, **93**, 878–886.
52 M. S. H. Al-Furjan, L. Shan, X. Shen, M. S. Zarei, M. H. Hajmohammad and R. Kolahchi, A review on fabrication techniques and tensile properties of glass, carbon, and Kevlar fiber reinforced polymer composites, *J. Mater. Res. Technol.*, 2022, **19**, 2930–2959.
53 T. P. Sathishkumar, M. Muralidharan, S. Ramakrishnan, M. R. Sanjay and S. Siengchin, Mechanical strength retention and service life of Kevlar fiber woven mat reinforced epoxy laminated composites for structural applications, *Polym. Compos.*, 2021, **42**, 1855–1866.
54 M. Y. M. Zaghloul, M. M. Y. Zaghloul and M. M. Zaghloul, Developments in polyester composite materials-An in-depth review on natural fibres and nano fillers, *Compos. Struct.*, 2021, **278**, 114698.